Analysis of the Imaging Realization of Frequency Modulated Continuous Wave Circular SAR

Gaowei Jia, **Wenge Chang**, **and Ruibin Tu**
College of Electronic Science and Engineering
National University of Defense Technology, Changsha, Hunan 410073, China

Abstract— Regarding the signal processing of frequency modulated continuous wave (FMCW) circular synthetic aperture radar (CSAR), the movement during the transmission of a pulse is considered to be one of the major problems. According to the Fourier-based imaging procedures of CSAR, the influence of intra-pulse movement is investigated and the corresponding correction method is presented. Numerical simulation tests verified the proposed correction method is feasible to remove the influence of the intra-pulse movement exactly.

1. INTRODUCTION

There has been increasing interest in frequency modulated continuous wave (FMCW) synthetic aperture radar (SAR) in the last years [1–3], which has led to the construction of several experimental systems. On the other hand, circular SAR (CSAR) has lately become of the hotspot in the field of SAR due to its characteristics like super-high resolution, three-dimensional imaging possibility, and all-aspect observation. Changing the acquisition geometry of FMCW SAR from a straight line to a circular trajectory may combine the advantages of both FMCW radar and CSAR.

As for the imaging processing of FMCW SAR, it is well known that the intra-pulse movement would introduce new range migration and affect the range cell migration correction (RCMC). Similarly, and it is found that the intra-pulse movement also leads to new range migration in the case of FMCW CSAR and further distorts the imaging results. [2] has verified that the modified BPA is feasible to focus the FMCW CSAR data very well. However, the modified BPA and its potential improvements encounter huge computation. To improve the imaging efficiency, the modified Fourier-based imaging procedures of FMCW CSAR is expected to be investigated.

2. THE SIGNAL MODEL OF CIRCULAR FMCW SAR

Let us refer to the imaging geometry of FMCW CSAR in Fig. 1.

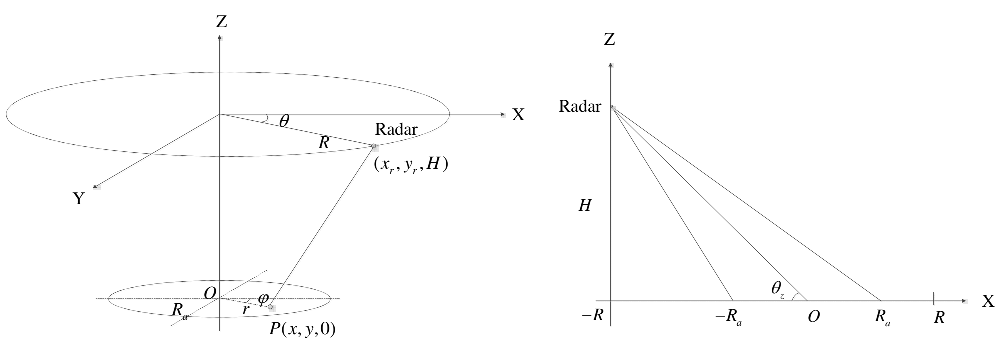

Figure 1: The imaging geometry of FMCW CSAR (a) 3-D view, (b) the side view.

Figure 1(a) stands for the imaging geometry of FMCW CSAR and Fig. 1(b) denote its side view. In Fig. 1(a), the SAR sensor moves along a circle with the radius of R, the velocity is v. $\theta \in [0, 2\pi]$ represents the aspect angle, 0 degree of θ stands for the positive x axis. O is the origin. The three dimensional (3-D) positions of the array phase center (APC) are (x_r, y_r, H), i.e., (R, θ, H) in the polar coordinates. During the movement of SAR sensor, the beam is always spotlighted on the flat observed scene (with a radius of R_a). P is an arbitrary off-centered target located in the observed area with the 3-D positions of $(x, y, 0)$, i.e., $(r, \phi, 0)$ in the polar coordinates. In Fig. 1(b), θ_z stands for the incident angle according to the origin. With $x_r = R\cos\theta$, $y_r = R\sin\theta$ and

$x = r\cos\varphi,\ y = r\sin\varphi$, the instantaneous range from the APC to P is

$$R_r(\theta) = \sqrt{R^2 + r^2 + H^2 - 2Rr\cos(\theta - \varphi)} \tag{1}$$

It is assumed that the angular velocity of radar is w, t denotes the time axis, t_m and $\hat{t}$ are the slow time and fast time, respectively. Based on the results in [2], we have:

$$R_r(\theta) \approx R_r(\theta_m) + \chi(\theta_m)\hat{t} \tag{2}$$

in which $\theta_m = wt_m$, $R_r(\theta_m) = \sqrt{R^2 + r^2 + H^2 - 2Rr\cos(\theta_m - \varphi)}$, and $\chi(\theta_m) = r\sin(\theta_m - \varphi)v/R_r(\theta_m)$. In (2), the term $\chi(\theta_m)\hat{t}$ denotes the new displacement introduced from the intra-pulse movement.

It is assumed that the transmitted linear modulated frequency (LFM) pulse. The intermediate frequency signal after residual video phase (RVP) filtering [4] is

$$S(\hat{t}, \theta_m) = \exp\left(-j\left(\frac{4\pi}{\lambda} + \frac{4\pi\gamma\hat{t}}{c}\right)R_r(\theta_m)\right)\exp\left(-j\frac{4\pi}{\lambda}\chi(\theta_m)\hat{t}\right) \tag{3}$$

Denoting $k = \frac{2\pi}{\lambda} + \frac{2\pi\gamma\hat{t}}{c}$, k represents the wavenumber in range. Then (3) could be rewritten as

$$S(k, \theta_m) = \exp(-j2kR_r(\theta_m))\exp\left(-j\frac{4\pi}{\lambda}\chi(\theta_m)\hat{t}\right) \tag{4}$$

Equation (4) is the expression of the received signal of FMCW CSAR in angle time domain. To obtain the 2-D spectrum of FMCW CSAR, the Fourier transform with respect to θ_m yields

$$S(k, \xi) = \int \exp(-j2kR_r(\theta_m))\exp\left(-j\frac{4\pi}{\lambda}\chi(\theta_m)\hat{t}\right)\exp(-j\xi\theta_m)d\theta_m \tag{5}$$

in which ξ stands for the wavenumber in the angular domain. In order to determine a closed form expression of $S(k, \xi)$, the principle of stationary phase (POSP) is used [5, 6]. The stationary point is achieved by solving the equation shown in (11).

$$\xi = -2kRr\frac{\sin(\theta_m - \varphi)}{\sqrt{\alpha^2 - 2\beta\cos(\theta_m - \varphi)}} \tag{6}$$

in which $\alpha^2 = R^2 + r^2 + H^2$, $\beta = Rr$. During the calculation of stationary points, the exponential term $\exp(j4\pi\chi(\theta_m)\hat{t}/\lambda)$ is ignored since the phase of which is much smaller than that of $\exp(-j2kR_r(\theta_m))$. Solving the Equation (11) yields two stationary points θ_1^* and θ_2^*, which follow the relationship shown in (12) and (13), respectively.

$$\cos(\theta_1^* - \varphi) = \frac{\xi^2 + \sqrt{\xi^4 - 4k^2\xi^2\alpha^2 + 16k^4\beta^2}}{4k^2\beta} \tag{7}$$

$$\cos(\theta_2^* - \varphi) = \frac{\xi^2 - \sqrt{\xi^4 - 4k^2\xi^2\alpha^2 + 16k^4\beta^2}}{4k^2\beta} \tag{8}$$

With the solutions from (7) and (8) we could obtain the 2-D spectrum of FMCW CSAR in the domain of (k, ξ), i.e.,

$$\begin{aligned} S(k, \xi) = \exp\Bigg\{ & -j\sqrt{4k^2\alpha^2 - 2\xi^2 - 2\sqrt{\xi^4 - 4k^2\xi^2\alpha^2 + 16k^4\beta^2}} \\ & + j\,|\xi|\cos^{-1}\left(\frac{\xi^2 + \sqrt{\xi^4 - 4k^2\xi^2\alpha^2 + 16k^4\beta^2}}{4k^2\beta}\right) - j\xi\varphi + j\frac{4\pi}{\lambda}\frac{\xi}{2kR}v\hat{t}\Bigg\} \\ & + \exp\Bigg\{-j\sqrt{4k^2\alpha^2 - 2\xi^2 + 2\sqrt{\xi^4 - 4k^2\xi^2\alpha^2 + 16k^4\beta^2}} \\ & + j\,|\xi|\cos^{-1}\left(\frac{\xi^2 - \sqrt{\xi^4 - 4k^2\xi^2\alpha^2 + 16k^4\beta^2}}{4k^2\beta}\right) - j\xi\varphi + j\frac{4\pi}{\lambda}\frac{\xi}{2kR}v\hat{t}\Bigg\} \end{aligned} \tag{9}$$

The expression shown in (9) represent the spectrum of FMCW CSAR in the slant plane, it is the basis for further imaging processing. In (9), the exponential term $\exp(j4\pi\xi v\hat{t}/2kR\lambda)$ is introduced from $\exp(-j4\pi\chi(\theta_m)\hat{t}/\lambda)$, i.e., from the intra-pulse continuous movement.

The main contributions of this section are the proposals of the signal model and the spectrum expression of FMCW CSAR. Equation (9) is the basis of the imaging processing of FMCW CSAR.

3. THE INFLUENCE AND REMOVAL OF THE INTRA-PULSE MOVEMENT

According to the spectrum of FMCW CSAR shown in (9), the phase term derived from the movement during the pulse is rewritten as

$$P(\hat{t},\xi) = \frac{4\pi}{\lambda}\frac{\xi}{2kR}v\hat{t} \tag{10}$$

$P(\hat{t},\xi)$ is considered as phase errors and may distort the final CSAR images. Firstly it is necessary to measure the relative variation of the phase error. Based on Equation (6), it is learnt that the absolute value of ξ has its maximum, i.e.,

$$|\xi| \leq 2kRr\frac{\sqrt{2\alpha^2 - 2\sqrt{\alpha^4 - 4\beta^2}}}{2\beta} \approx 2kr\cos\theta_z \tag{11}$$

where $|\cdot|$ denotes the absolute value. In addition, it is known $k = 2\pi/\lambda + 2\pi\gamma\hat{t}/c$ and $\hat{t} \in [0, T_p]$, T_p is the time duration of LFM. Thus the relative maximum phase variation within the whole spectrum support domain is

$$P_{\max} = 2\frac{4\pi}{\lambda}\frac{r\cos\theta_z}{R}vT_p \tag{12}$$

It is learnt that the value of $P_{\max}$ increases against with r, denoting the target with larger radius would suffer higher phase errors. When $P_{\max}$ is larger than $\pi/4$, distortion of CSAR image may appear thus proper operation is expected to remove $P(\hat{t},\xi)$ exactly. To have a better insight of the phase error, quantitative calculation is carried out. The parameters according to an X-band FMCW CSAR are adopted and listed in Table 1.

Table 1: parameters.

Carrier frequency	10 GHz	Radius of the circular track	1000 m
Bandwidth	600 MHz	Height of track	500 m
Pulse duration	4 ms	Velocity of carrier	40 m/s

During the simulation test, several target points is used. Taking one target (40 m, 0 m) for example, the corresponding phase history and the variation of $P(\hat{t},\xi)$ are figured out and shown in Fig. 2.

Figure 2(a) stands for the phase history according to target (40 m, 0 m), in which assumes that the radar is stationary during the transmission of a sweep. Correspondingly, Fig. 2(b) stands for the phase history which has taken the intra-pulse movement into accounted. The mixing between the phase history shown in Figs. 2(a) and (b) yields the phase errors derived from the intra-pulse movement, as shown in Fig. 2(c). Fig. 2(d) represents the phase errors calculated with Equation (12). Compared Fig. 2(c) with Fig. 2(d), it is found that they matched each other well, denoting the signal model analysis in Section 2 is correct. In addition, it is seen that the relative maximum phase error at $r = 40$ m is 4.79 rad, which is larger than $\pi/4$ and will degrade the final FMCW CSAR images.

Fortunately, it is learnt that $\exp(j4\pi\xi v\hat{t}/2kR\lambda)$ has no dependence on the position of target, thus it is space-invariant and easy to be removed by matched filtering. Specifically, the matched filter is defined as

$$H_r(k,\xi) = \exp\left(-j\frac{4\pi}{\lambda}\frac{\xi}{2kR}v\hat{t}\right) \tag{13}$$

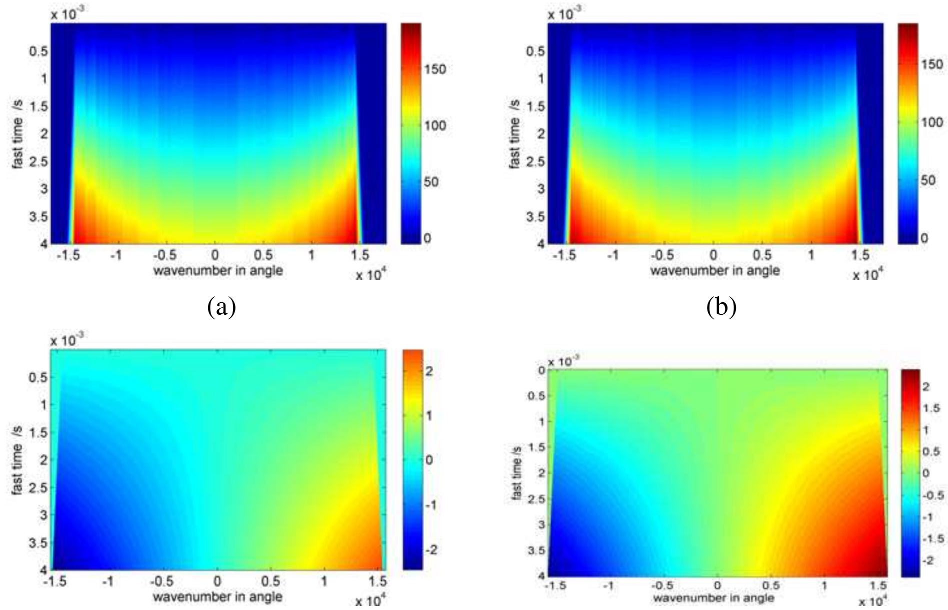

(a) (b) (c) (d)

Figure 2: The phase error analysis, (a) phase history without intra-pulse movement, (b) phase history with intra-pulse movement, (c) the extracted phase error, (d) the phase error calculated by (12).

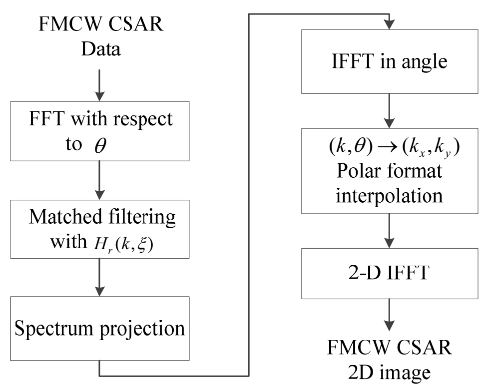

Figure 3: The modified Fourier-based imaging flow of FMCW CSAR.

After the matched filtering, the spectrum of FMCW CSAR is same with that of pulsed CSAR. Based on the former analysis about CSAR in [5], the Fourier-based imaging flow of FMCW CSAR is given in Fig. 3.

In Fig. 3, the correction procedure is performed by phase multiplication, to the benefit of high efficiency. As for the spectrum projection operation, it is independent on the removal of intra-pulse movement, although it is another important procedure within the imaging flow of FMCW CSAR. The main contributions of this section contain: On one hand, it is learnt that the intra-pulse movement would introduce phase errors, and it is necessary to remove the phase error properly once the relative variation of which is larger than $\pi/4$. On the other hand, the corresponding correction method is proposed to remove the influence of intra-pulse movement.

4. SIMULATION TESTS

Simulation test is carried out in this section and the parameters are same with that listed in Table 1. During the imaging processing, the modified BPA [2] is used to produce ideal imaging results. Figs. 4(a) and (d) stand for the imaging result of FMCW CSAR data processed by Fourier-based imaging methods without and with the correction operation, respectively. Fig. 4(b) denotes the imaging results processed with the modified BPA. Fig. 4(c) denotes the CSAR spectrum in ground plane.

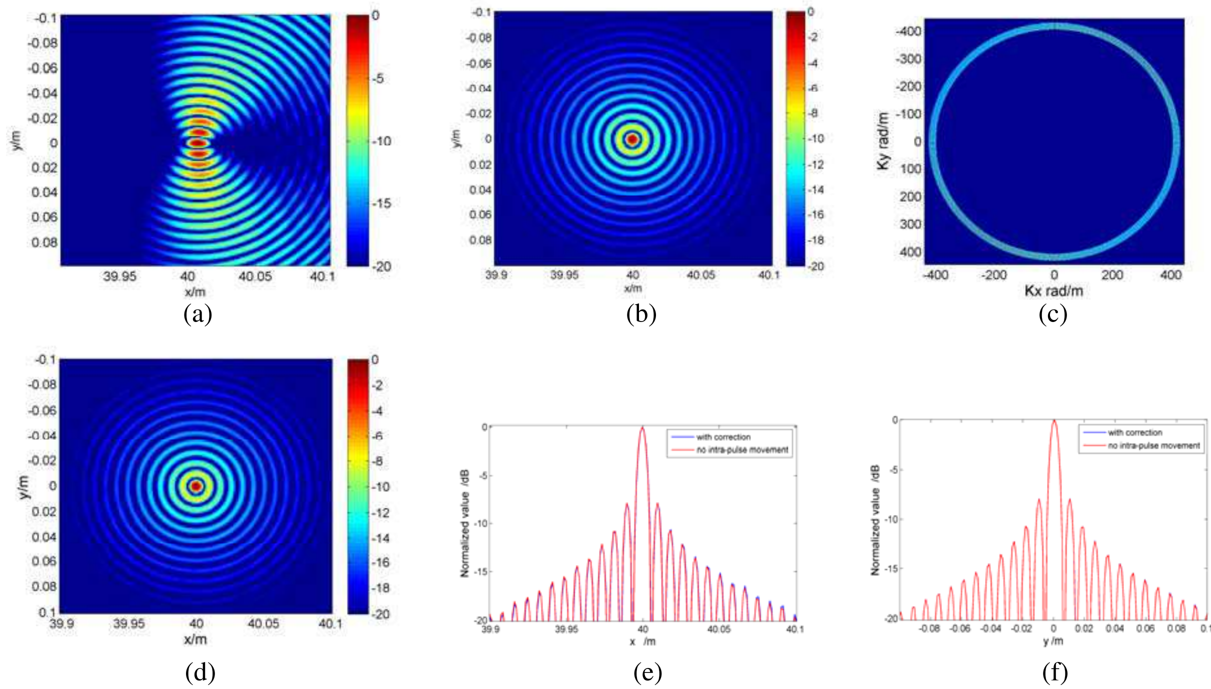

Figure 4: The imaging result with simulated CSAR data, (a) processed without the correction of intra-pulse movement, (b) processed with modified BPA, (c) the spectrum after polar formatting resampling, (d) processed with the proposed method, (e) and (f) denote the profiles.

According to the PSFs shown in Figs. 4(b) and (d), the corresponding profiles in x and y are shown in Figs. 4(e) and (f), respectively. Specifically, the blue and red curves stand for the profiles processed with the proposed improvement and the modified BPA, respectively. It is seen that the results processed with the proposed method coincides the ideal results very well, denoting again that the first proposed improvement is valid and is helpful to figure out the well-focused FMCW CSAR image.

5. CONCLUSION

Removing the influence of intra-pulse movement is proposed in this paper. During the Fourier-based imaging processing of FMCW CSAR, the movement within the pulse leads to the emergence of phase errors and eventually distorts the final image. Correspondingly, a modified Fourier-based imaging method is proposed for FMCW CSAR.

REFERENCES

1. Jia, G. W. and W. G. Chang, "Study on the improvements for the high-resolution frequency modulated continuous wave synthetic aperture radar imaging," *IET Radar, Sonar and Nav.*, 2014.
2. Jia, G. W. and W. G. Chang, "Modified back projection reconstruction for circular FMCW SAR," *International Radar Conference 2014*, Oct. 13–17, 2014.
3. Palm, S., A. Maresch, and U. Stilla, "Investigation on circular mapping by fmcw-sar on small airplanes," *Int. Arch. Photogramm. Remote Sens. Spatial Inf. Sci.*, XL-1/W1, 281–286, May 21–24, 2013.
4. Meta, A., P. Hoogeboom, and L. P. Ligthart, "Signal processing for FMCW SAR," *IEEE Trans. Geosci. Remote Sens.*, Vol. 45, No. 11, 3519–3532, 2007.
5. Soumekh, M., *Synthetic Aperture Radar Signal Processing with Matlab Algorithms*, John Wiley & Sons, Inc., New York, NY, 1999.
6. Carrara, W. G., R. S. Goodman, and R. M. Majewski, *Spotlight Synthetic Aperture Radar Signal Processing Alogrithms*, Artch House, Boston, London, 1995.